

This article was downloaded by: [Rikagaku Kenkyusho MZ]

On: 18 September 2008

Access details: Access Details: [subscription number 791272761]

Publisher Taylor & Francis

Informa Ltd Registered in England and Wales Registered Number: 1072954 Registered office: Mortimer House, 37-41 Mortimer Street, London W1T 3JH, UK



## Journal of Modern Optics

Publication details, including instructions for authors and subscription information:

<http://www.informaworld.com/smpp/title-content=t713191304>

### Wavelength dependence of high-harmonic generation from ultrashort pulses

K. Schiessl<sup>a</sup>; K. L. Ishikawa<sup>bc</sup>; E. Persson<sup>a</sup>; J. Burgdörfer<sup>a</sup>

<sup>a</sup> Institute for Theoretical Physics, Vienna University of Technology, Vienna, Austria <sup>b</sup> Department of Quantum Engineering and Systems Science, Graduate School of Engineering, University of Tokyo, Tokyo, Japan <sup>c</sup> PRESTO (Precursory Research for Embryonic Science and Technology), Japan Science and Technology Agency, Saitama, Japan

Online Publication Date: 01 September 2008

**To cite this Article** Schiessl, K., Ishikawa, K. L., Persson, E. and Burgdörfer, J.(2008)'Wavelength dependence of high-harmonic generation from ultrashort pulses',*Journal of Modern Optics*,55:16,2617 — 2630

**To link to this Article:** DOI: 10.1080/09500340802130787

**URL:** <http://dx.doi.org/10.1080/09500340802130787>

PLEASE SCROLL DOWN FOR ARTICLE

Full terms and conditions of use: <http://www.informaworld.com/terms-and-conditions-of-access.pdf>

This article may be used for research, teaching and private study purposes. Any substantial or systematic reproduction, re-distribution, re-selling, loan or sub-licensing, systematic supply or distribution in any form to anyone is expressly forbidden.

The publisher does not give any warranty express or implied or make any representation that the contents will be complete or accurate or up to date. The accuracy of any instructions, formulae and drug doses should be independently verified with primary sources. The publisher shall not be liable for any loss, actions, claims, proceedings, demand or costs or damages whatsoever or howsoever caused arising directly or indirectly in connection with or arising out of the use of this material.

## Wavelength dependence of high-harmonic generation from ultrashort pulses

K. Schiessl<sup>a\*</sup>, K.L. Ishikawa<sup>b,c†</sup>, E. Persson<sup>a</sup> and J. Burgdörfer<sup>a</sup>

<sup>a</sup>Institute for Theoretical Physics, Vienna University of Technology, Vienna, Austria;

<sup>b</sup>Department of Quantum Engineering and Systems Science, Graduate School of Engineering, University of Tokyo, Tokyo, Japan; <sup>c</sup>PRESTO (Precursory Research for Embryonic Science and Technology), Japan Science and Technology Agency, Saitama, Japan

(Received 19 March 2008; final version received 14 April 2008)

We investigate the dependence of the intensity of radiation due to high-harmonic generation (HHG) as a function of the wavelength  $\lambda$  of a few-cycle driver field. Superimposed on a smooth power-law dependence observed previously, strong and rapid fluctuations on a fine  $\lambda$  scale are observed. The origin of these fluctuations can be identified in terms of quantum path interferences with several orbits significantly contributing. The dependence on the pulse shape and pulse length of the driver is analyzed. We discuss the relation to well-known channel closing effects with emphasis on effects of the ultrashort duration of the pulse.

**Keywords:** high harmonic generation; driver wavelength; quantum path interference

### 1. Introduction

High harmonic generation (HHG) represents a versatile and highly successful avenue towards an ultrashort coherent light source covering a wavelength range from the vacuum ultraviolet to the soft X-ray region [1]. This development has led to new research areas, such as attosecond science [2,3] and nonlinear optics in the XUV region [4,5]. The fundamental wavelength  $\lambda$  used in most of existing HHG experiments is in the near-visible range ( $\sim 800$  nm). The cutoff law for the harmonic spectrum  $E_c = I_p + 3.17U_p$  ( $I_p$  is the ionization potential of the target atom,  $U_p = F_0^2/4\omega^2$  is the ponderomotive energy, and  $F_0$  is laser electric field strength), suggests that a longer fundamental wavelength would be advantageous to extend the cutoff to higher photon energies, since  $U_p$  increases quadratically with  $\lambda$ . There is an increasing interest in the development of high-power mid-infrared ( $\sim 2$   $\mu$ m) laser systems, e.g. based on optical parametric chirped pulse amplification. Along those lines the dependence of the HHG yield on  $\lambda$  has become an issue of major interest. Recently, Tate et al. [6] have reported on the dependence of the harmonic (HHG) yield between 800 nm and 2  $\mu$ m calculated with the time-dependent Schrödinger equation (TDSE) for Ar and a strong-field approximation (SFA) for He.

---

\*Corresponding author. Email: klaus@concord.itp.tuwien.ac.at

†Current address: Research Program for Computational Science, RIKEN, Wako, Saitama, Japan.

They found the yield to be described by a power-law  $\propto \lambda^{-x}$  with  $5 \leq x \leq 6$ . More recently, we have investigated the  $\lambda$  dependence on the level of single-atom response for H and Ar by numerically solving the time-dependent Schrödinger equation [7]. While we could confirm the overall scaling  $\propto \lambda^{-x}$ , the harmonic yield was found not to depend smoothly on the fundamental wavelength, but to exhibit surprisingly rapid oscillations with a period of 6–20 nm depending on the wavelength region. A semiclassical analysis based on the SFA has revealed that the rapid oscillations are due to the interference of five to 10 different rescattering trajectories [7].

Oscillations of the HHG yield have been previously reported in terms of the dependence on the intensity of the driver  $I_0 \propto F_0^2$ , both experimentally [8,9] and theoretically [10,11]. Borca et al. [11] and Milošević and Becker [10] have shown that HHG is enhanced at channel closings (CC), i.e. if

$$R = \frac{I_p + U_p}{\omega} \quad (1)$$

is an integer. Most of these theoretical studies employed zero-range potentials or the SFA which both neglect the influence of the long-range potential on the ionized electron.

In the present communication we extend our investigation to the wavelength and intensity dependence of the HHG yield with the emphasis on the pulse shape and pulse duration dependence. Even though our primary focus is on ultrashort few-cycle pulses, we also analyze the relation of the interference oscillations as a function of the wavelength with those as a function of the intensity. Similarities and differences will be discussed. Furthermore, we investigate the dependence on the atomic species and on the form of the atomic potential, reflecting effects of the atomic potential beyond the SFA.

The present paper is organized as follows. Section 2 summarizes the two complementary integration schemes employed for a full numerical solution of the TDSE. In Section 3 we discuss the overall wavelength dependence as well as small-scale variations at a fixed value of fundamental intensity. We analyze the origin of rapid oscillations of the HHG yield based on the SFA in Section 4. The dependence of the latter on the pulse shape and on the pulse length is discussed in Section 5. In Section 6 we extend our discussion to the wavelength and intensity dependence, in particular, as a function of the parameter  $R$  (Equation (1)) which is frequently used to describe channel closings. Conclusions are given in Section 7. Atomic units are used throughout the paper unless otherwise stated.

## 2. Numerical method

We solve the atomic time-dependent Schrödinger equation (TDSE) in the length gauge for a linearly polarized laser field with central wavelength  $\lambda_c = 2\pi c/\omega$ ,

$$i \frac{\partial}{\partial t} \psi(\mathbf{r}, t) = \left[ -\frac{1}{2} \nabla^2 + V_{\text{eff}}(r) + z F(t) \right] \psi(\mathbf{r}, t), \quad (2)$$

where  $F(t) = F_0 f(t) \sin(\omega t)$  denotes the laser electric field,  $f(t)$  is the envelope function and  $V_{\text{eff}}(r)$  is the atomic potential. For H,  $V_{\text{eff}}(r)$  is the bare Coulomb potential while for Ar we employ a model potential [12] within the single-active electron approximation which reproduces the binding energy to an accuracy of typically  $\approx 10^{-3}$ .

We employ two complementary methods to solve Equation (2) in order to establish reliable and consistent results.

In the first method, Equation (2) is numerically integrated using the alternating direction implicit (Peaceman–Rachford) method [13] with a uniform grid spacing  $\Delta r$  of  $6.25 \times 10^{-2}$  au. The time step  $\Delta t$  is 1/16,000 of an optical cycle for 800 nm wavelength, i.e.  $6.9 \times 10^{-3}$  au. This algorithm is accurate to the order of  $\mathcal{O}(\Delta t^3)$ . In the second method, the TDSE is integrated on a finite grid by means of the pseudo-spectral method [14] which is also accurate to the order of  $\mathcal{O}(\Delta t^3)$ . It allows for time-steps of the order of 0.1 atomic units. The  $r$  coordinate is discretized within the interval  $[0, r_{\max}]$  with a non-uniform mesh point distribution. The innermost grid point is typically as small as  $2.5 \times 10^{-4}$  au, enabling an accurate description near the nucleus. A smooth cutoff function is multiplied at each time-step to avoid spurious reflections at the border  $r_{\max}$ , while an analogous cutoff function prevents reflections at the largest resolved energy  $E_{\max}$ . Deeply bound, occupied states supported by the model potential are dynamically blocked during the time evolution by assigning a phase corresponding to an unphysically large and positive energy eigenvalue [15]. We calculate the dipole acceleration  $\ddot{d}(t) = -\partial_t^2 \langle z(t) \rangle$  with  $z = r \cos\theta$ , employing the Ehrenfest theorem through the relation  $\ddot{d}(t) = \langle \psi(\mathbf{r}, t) | \cos\theta/r^2 - F(t) | \psi(\mathbf{r}, t) \rangle$  [14], in which the second term can be dropped as it does not contribute to the HHG spectrum.

### 3. Global $\lambda$ dependence

For the analysis of the large-scale  $\lambda$  dependence we adopt the laser parameters of [6], with a fixed peak intensity of  $1.6 \times 10^{14}$  W cm $^{-2}$ , a variation of  $\lambda$  between 800 nm and 2  $\mu$ m, and an envelope function  $f(t)$  corresponding to an eight-cycle flat-top sine pulse with a half-cycle turn-on and turn-off. The HHG yield, defined as radiated energy per unit time [7], is determined by integrating over an energy window  $\Delta E$ ,

$$\Delta Y = \frac{1}{3c^3} \int_{20 \text{ eV}}^{50 \text{ eV}} |a(\omega')|^2 d\omega'. \quad (3)$$

Note that the energy window  $\Delta E$  of the output radiation (here 20 to 50 eV) is kept constant when analyzing  $\Delta Y$  as a function of  $\lambda$ . Calculated on a coarse mesh in  $\lambda$  with a spacing of 50 nm (Figure 1),  $\Delta Y$  falls off with a power law,  $\Delta Y \propto \lambda^{-x}$  ( $x \approx 4.8$ – $5.5$ ) for H and Ar [7], in qualitative agreement with [6]. The two alternative integration algorithms employed agree well with each other. Small discrepancies near 2  $\mu$ m are due to the difference in grid spacing and can be controlled by changes in the spacing near the origin. A power law ( $x \approx 5$ ) results from the combination of two effects: the spreading of the returning wavepacket would give  $x = 3$  [16] for the overall yield. The spread of the HHG yield over a wider spectral range with an upper cutoff growing as  $E_c \propto \lambda^2$  leads to an additional decrease of yield  $\propto \lambda^{-2}$  within the fixed window  $\Delta E$  (see Equation (3)). In fact, when increasing the upper integration limit in Equation (3) to the cutoff energy  $E_c$ , the exponent of the power law diminishes and reaches  $x \approx 3.5$  to 3.6 for Ar and H, in closer agreement with [16].

A more detailed look at Figure 1 reveals the remarkable feature that the harmonic yield does not vary smoothly with  $\lambda$  as may have been anticipated in previous work [6], but strongly fluctuates. Slight change in fundamental wavelength may lead to variations of the

yield by a factor of 2 to 6. Such rapid fluctuations imply that a reliable  $\lambda$  dependence can only be established by employing a much finer resolution. The fluctuations are not specific to hydrogen but appear for argon as well [7].

#### 4. Small-scale variations and path interference

Many features of HHG can be intuitively and even quantitatively explained in terms of returning classical (or quantum) trajectories [16,17] underlying the semiclassical three step model [18]. The main contribution to the HHG spectrum comes from those electronic paths that correspond to returning trajectories ionized at a certain time  $t_i$  and recombining with the parent ion at a later time  $t_f$ . Interference oscillations are controlled by the evolution phase, the semiclassical action of the path  $P$ , reading

$$S_P(t_i, t_f) = \int_{t_i}^{t_f} \frac{(p + A(t'))^2}{2} dt' + g \cdot I_p(t_f - t_i). \quad (4)$$

$I_p$  is the ionization potential (binding energy) of the atom and  $A(t)$  the laser vector potential defined by  $A(t) = -\int_t^\infty F(t') dt'$ .  $p$  is the canonical momentum of the returning trajectory. The empirical correction factor  $g$  (here  $g = 1.3$ ) has been frequently introduced to account for effects of an ‘effective’ threshold or binding energy when comparing with full TDSE solutions in the case of quantum path interference [19,20].

The time-dependent dipole moment  $d(t)$  is expressed as [21]

$$d(t_f) = \sum_{P(t_i)} b_{\text{ion}}(t_i) \exp[-iS_P(t_i, t_f)] c_{\text{rec}}(t_f) + c.c., \quad (5)$$

i.e. a sum over classical paths  $P$  that start at the moment of tunnel ionization  $t_i$  with amplitude  $b_{\text{ion}}(t_i)$ , evolve in the laser field  $-\exp[-iS_P(t_i, t_f)]$  – and recombine upon

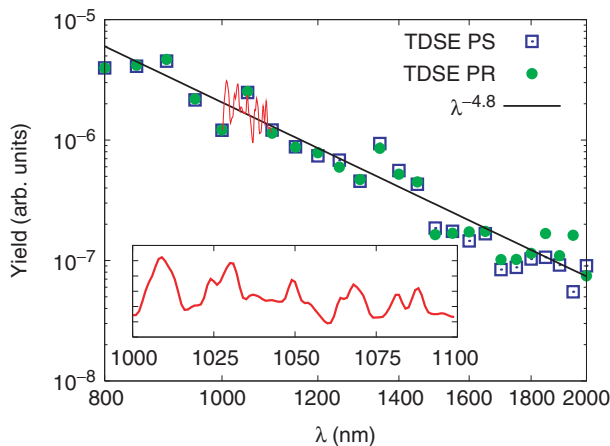


Figure 1. Integrated harmonic yield  $\Delta Y$  for hydrogen between 20 and 50 eV as a function of  $\lambda$  calculated on a coarse mesh with  $\Delta\lambda = 50$  nm. ●, Peaceman-Rachford method; □, pseudo-spectral method. Solid line: fit  $\Delta Y \propto \lambda^{-x}$ . The inset provides a zoom near 1  $\mu\text{m}$ . (The color version of this figure is included in the online version of the journal.)

rescattering at the core at time  $t_f$  with the amplitude  $c_{\text{rec}}(t_f)$ . Within this model, the dependence on the envelope function  $f(t)$  is explicitly included through the number and relative weight of returning trajectories contributing to the harmonic emission at a given frequency. For ultrashort few-cycle pulses this number is limited.

When including between five and 10 returning paths, the semiclassical calculation can reproduce the modulation depth, modulation frequency, and the approximate phase of the  $\lambda$  oscillations reasonably well, thus unambiguously establishing the quantum path interference as the origin of the fluctuations (see Figure 2(b)). Full convergence is only reached when up to ten trajectories are included. Setting  $g = 1.0$  the standard SFA result of predicting enhancements near channel closing is recovered, but at the price of an unwanted shift of the oscillations compared to the TDSE data.

In the case of Ar (Figure 2(c)), convergence also for small sub-peaks (e.g. at 1934, 1941, and 1947 nm) is reached after 10–12 trajectories. The visibility of contributions of multiple-returning trajectories with excursion times in the order of six half-cycles highlights the importance of such trajectories even in few-cycle pulses. Clear indications of the significance of such trajectories has recently also been found by Tate et al. in their analysis of the wavelength dependence of the HHG yield on a large  $\lambda$  scale [6].

We emphasize the remarkable variation on a fine  $\lambda$  scale for an ultrashort pulse. An ultrashort few-cycle pulse is characterized by a central wavelength  $\lambda_c$  and a Fourier broadening  $\Delta\lambda$ . In the present case,  $\Delta\lambda/\lambda_c$  is of the order of 20%. The rapid variations of the harmonic yield occur on a scale  $\delta\lambda$  much smaller than the Fourier width of the pulse. This finding, at a first glance surprising, is a direct consequence of the quantum path interference. It follows from the existence and the fixed spacing in between discrete points in time – controlled by  $\lambda_c$  – at which electronic trajectories are launched. As long as the few-cycle pulse permits the generation of a set of a few quantum paths in subsequent half-cycles, the overall temporal characteristics of the driver pulse is of minor importance, though the latter will influence the detailed shape of the interference pattern. A more detailed discussion of the dependence on the particular choice of the envelope function  $f(t)$  will be given in Section 5.

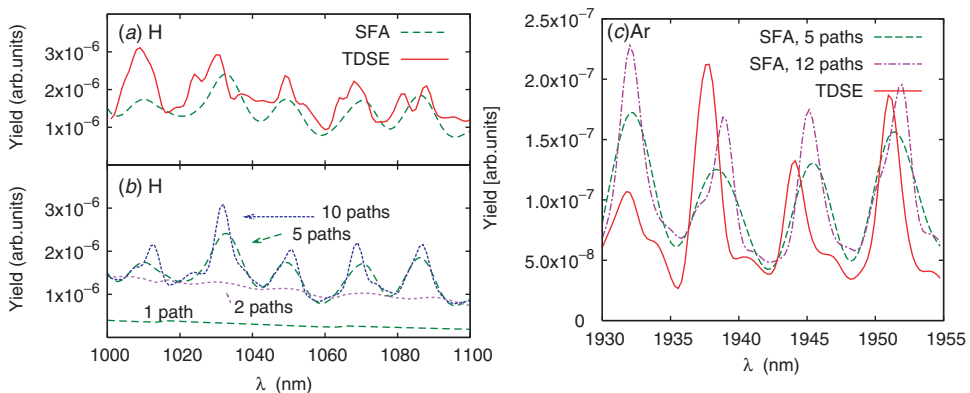


Figure 2. Variation of the integrated harmonic yield  $\Delta Y$  in a narrow range of  $\lambda$ , comparison of the SFA with results from the TDSE: (a) and (b) hydrogen near 1  $\mu\text{m}$ ; (c) argon near 2  $\mu\text{m}$ . (The color version of this figure is included in the online version of the journal.)

Expressed in terms of  $\lambda$ , the modulation period of the harmonic yield  $\delta\lambda$  is a function of the central wavelength  $\lambda_c$  itself. It is about 20 nm near 1  $\mu\text{m}$  wavelength and approaches  $\approx 6$  nm near a wavelength of 2  $\mu\text{m}$  (Figure 3). The scaling of  $\delta\lambda$  with  $\lambda$  can be estimated by a variation of semiclassical action in Equation (4) with  $\delta\lambda$  to be  $\propto \lambda^{-2}$  [7], which predicts the modulation length remarkably well (see Figure 3). The  $\lambda^{-2}$  dependence can, equivalently, also be deduced from the ‘channel closing’ picture discussed below in more detail (see Section 6).

## 5. Pulse length and pulse shape dependence

### 5.1. Pulse length dependence

The influence of the pulse length on the  $\lambda$  dependence of the harmonic yield can be observed in Figure 4. As might have been expected, the amplitude of the oscillations decreases with decreasing pulse length when long, multiple-returning electron trajectories are suppressed. On the other hand, for longer pulses the amplitude increases but evolves locally non-monotonically. For example, in the double peak structure visible in the yield oscillation of the eight cycles flat-top pulse (near 1030, 1050, and 1070 nm), the left subpeak grows and forms a sharp spike, while other subpeaks might even decrease. One can consider the results for a 16-cycle, flat-top pulse to be approximately ‘converged’ with respect to the pulse length. At the intensity considered, the ionization yield reaches already about 63%. Therefore, contributions of further cycles (in a longer pulse) are expected to be negligible because of ground-state depletion. SFA calculations incorporating ground-state depletion (i.e. the model described in Equation (5) and [21]) show a very similar behavior, confirming the appearance of a maximum number of quantum paths contributing due to ionization.

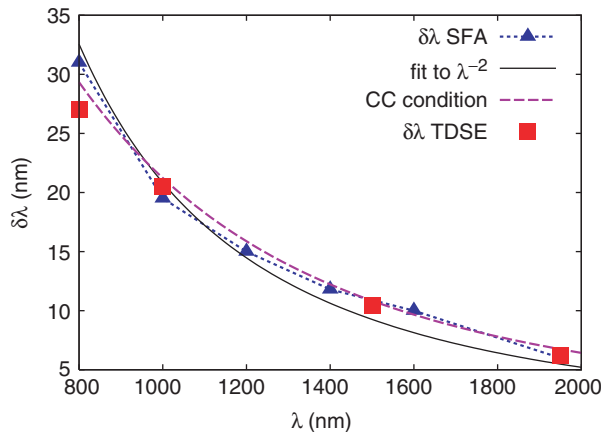


Figure 3. Variation of the modulation period  $\delta\lambda$  with the driver's central wavelength  $\lambda_c$  for hydrogen. ■, TDSE; ▲, SFA. Solid line:  $\lambda^{-2}$  scaling, dashed: channel closing condition (Equation (7)). (The color version of this figure is included in the online version of the journal.)

## 5.2. Pulse shape dependence

The full solution of the TDSE allows one to explore in detail the dependence of the harmonic yield on the shape of the envelope function  $f(t)$ , keeping in the following the effective duration of the pulse approximately constant. In Figure 5, oscillations originating from driving pulses with a ‘smooth’ envelope such as a  $\sin^2$ -pulse ( $f(t) = \sin^2(t\pi/\tau_{\text{tot}})$ ) with

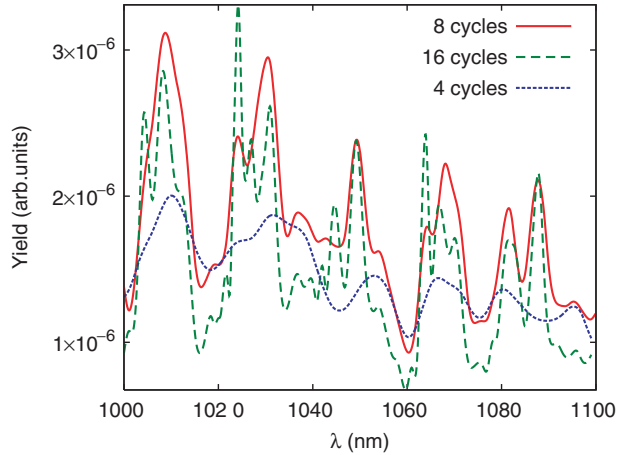


Figure 4. Fluctuations of the harmonic yield  $\Delta Y$  for hydrogen and different pulse durations as a function of  $\lambda$ . Solid, dashed, and dotted curves correspond to a total duration of 8, 16, and 4 cycles, respectively. Other pulse parameters are the same as in Figure 1. (The color version of this figure is included in the online version of the journal.)

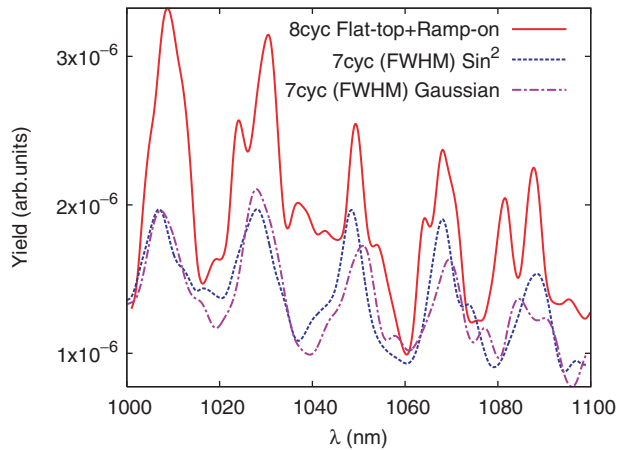


Figure 5. Fluctuations of the harmonic yield  $\Delta Y$  as a function of the fundamental wavelength  $\lambda$  for hydrogen. Solid: 8 cycles flat-top with a  $1/2$  ( $1/2$ ) cycle ramp on (off), dotted: 14 cycles  $\sin^2$  pulse with effectively  $\tau_p = 7$  cycles (FWHM) contributing, dash-dotted: 16 cycles Gaussian with a FWHM of  $\tau_p = 7$  cycles. Other pulse parameters are the same as in Figure 1. (The color version of this figure is included in the online version of the journal.)

$t \in [0, \tau_{\text{tot}}]$ ) or a Gaussian pulse ( $f(t) = \exp(-t^2/4 \ln 2 / \tau_p^2)$  with  $t \in [-\tau_{\text{tot}}/2, \tau_{\text{tot}}/2]$ ) are depicted along with the flat-top pulse. Qualitatively, the results for the flat-top pulse are recovered: the oscillations feature roughly the same modulation period with maxima near the same central wavelength. Remarkably, even the ratio of a maximum to a neighboring minimum remains in the same order of magnitude, namely about 2, although the absolute yield is somewhat lower. It should be noted that all pulses in Figure 5 have the same *effective* pulse length given by the full width at half maximum (FWHM), to which the harmonic yield (that is proportional to the radiated energy per time) is normalized here. For a  $\sin^2$ -pulse  $\tau_p = \tau_{\text{tot}}/2$ . For a Gaussian pulse,  $\tau_p$  is the FWHM of the Gaussian  $f(t)$ , while for the flat-top it is the full duration disregarding the ramp on (off). Overall, the influence of pulse shape is observed to be moderate, as long as the effective pulse length that determines the maximal number of contributing trajectories is kept fixed.

However, changing the number of contributing trajectories can lead to distinct changes even when just one additional cycle is added. This is illustrated in Figure 6 where a qualitative change of the interference pattern is observed by going from a  $\sin^2$ -pulse with  $\tau_p = 7$  to one with  $\tau_p = 8$  cycles. Remarkably, such qualitative changes do not appear for a flat-top pulse (see discussion in Section 5.1). The SFA model accounting for the interference of trajectories supported by the given pulse envelope (Equation (5)) is able to correctly reproduce this behavior.

## 6. Relation to channel closing interferences

### 6.1. Wavelength and intensity dependence

Interference of multiple quantum paths has previously been studied in the context of the intensity dependence of the harmonic yield [10,11]. Using a Floquet theory for

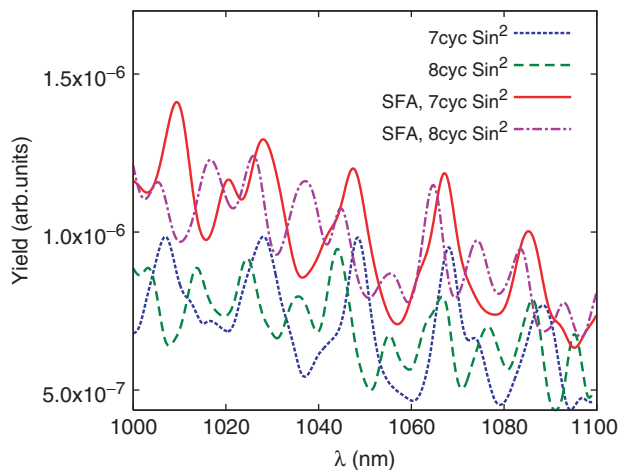


Figure 6. Fluctuations of the harmonic yield  $\Delta Y$  as a function of the fundamental wavelength  $\lambda$  for hydrogen. Dashed: 16 cycles  $\sin^2$  with a FWHM of  $\tau_p = 8$  cycles, dotted: 14 cycles  $\sin^2$ ,  $\tau_p = 7$  cycles, solid: SFA based on classical trajectories with up to 20 paths,  $\tau_p = 7$  cycles, dash-dotted: same as the latter, but  $\tau_p = 8$  cycles. Other pulse parameters are the same as in Figure 1. (The color version of this figure is included in the online version of the journal.)

a zero-range potential and the strong-field approximation, Borca et al. [11], and Milošević and Becker [10] have shown that the HHG yield exhibits resonance-like enhancements when the  $n$ -photon ionization channel is closed with increasing intensity. Very recently, first experimental evidence for the interference between the short and long paths was presented [8] in the intensity dependence of the HHG yield. Expressed in terms of the parameter  $R$  (Equation (1)), resonance peaks are expected at integer values of  $R$  [10,11]. Since the pulse has been assumed to have constant field strength and to be monochromatic ( $f(t) = 1$ ) in these studies, it may contain a very large (in fact, up to an infinite) number of trajectories giving rise to sharp structures near the channel closing resonance. This is obviously qualitatively different from the present case of few-cycle pulses, where the number of trajectories is strictly limited by the pulse shape and thus by the Fourier broadening. Nevertheless, the appearance of a large number of interfering trajectories suggests an interrelation to the case of rapid oscillations in the wavelength dependence. To clarify this relation we analyze the HHG yield as a function of  $R$  which, in turn, is also a function of  $\lambda$ , namely

$$R(\lambda) = \frac{I_p + U_p(\lambda)}{\omega} = \frac{(I_p + \lambda^2 I / 16\pi^2 c^2) \lambda}{2\pi c}. \quad (6)$$

Note, however, the intensity and hence the ponderomotive energy is strongly time dependent for a few-cycle pulse. For the following discussion of the HHG yield as a function of  $R$  (Equation (6)) we employ the maximum intensity  $I_0$  at the temporal peak of the envelope function, although temporal intensity averaging is, from the start, included in the HHG spectrum for an ultrashort driving pulse.

Figure 7 displays dependence on the central wavelength for hydrogen around  $\lambda = 1 \mu\text{m}$  expressed by  $\lambda$  for different values of peak intensity  $I_0$ . The yield exhibits rapid fluctuations both when the wavelength is varied at a fixed value of  $I_0$ , as well as a function of  $I_0$  when  $\lambda_c$  is kept constant. Expressed in terms  $R$  (Figure 8(a)) the maxima in the yield at each individual value of  $I_0$  overlap, showing a common functional dependence. This observation suggests that the wavelength and intensity dependence of the HHG yield can be discussed as a function of  $R$  instead of  $\lambda_c$ . Not only the peak positions but also detailed structures of the dependence on  $\lambda_c$  are quite robust against the variation of  $I_0$ , when expressed in terms of  $R$ .

Results for argon (Figure 8(b)) show a similar behavior, indicating the applicability of the parameter  $R$  independent of the atomic species. Interference peaks appear with spacings given by  $\delta R = 1$ . However, the peaks do not appear at integer values of  $R$ . For monochromatic (long) pulses with constant intensity such shifts have been attributed to the appearance of effective thresholds [19,20,22]. Corrections to the CC condition (Equation (1)) have been proposed to account for excited states that are missing in SFA models [19,20,22]. Qualitatively, such corrections have the same effect as the parameter  $g$  introduced in Equation (4). The spacing  $\delta R$  is closely related to the spacing  $\delta\lambda$  in the wavelength dependence of the peak positions. This relation can be made explicit with the help of the following consideration. We first note that the semiclassical action  $S_P$  in Equation (4) has its largest contribution from the  $A(t)^2$  term in the strong field case and can be approximated by  $S_P \approx (U_p + I_p)\tau_f = R\omega\tau_f$  where  $\tau_f = t_f - t_i$  is the flight time of the electron trajectory [17], which is approximately a multiple of the half laser cycle  $\pi/\omega$ .

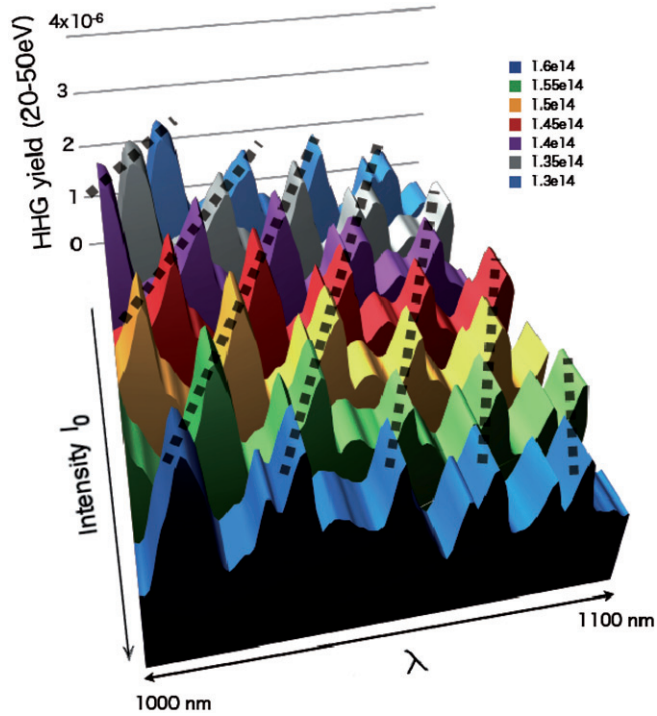


Figure 7. TDSE-calculated integrated harmonic yield  $\Delta Y$  between 20 and 50 eV as a function of the central wavelength  $\lambda_c$  and for different values of peak intensity  $I_0$  indicated in the figure. Dotted lines roughly connect maxima for different values of intensity, following lines of constant values of  $R$ . (The color version of this figure is included in the online version of the journal.)

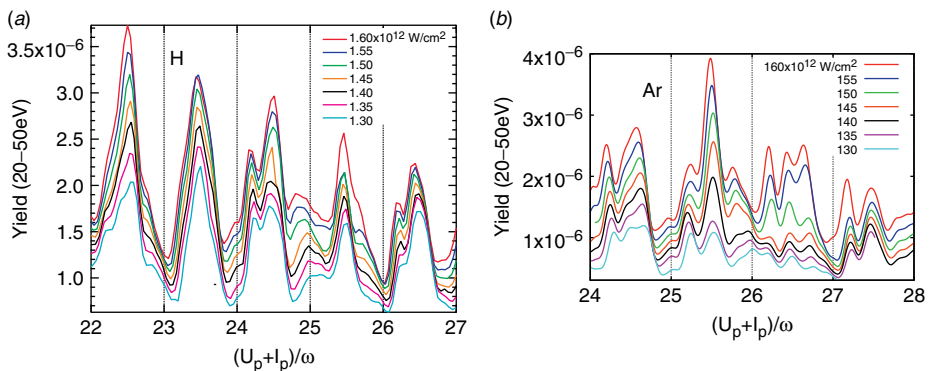


Figure 8. Fluctuations of the harmonic yield  $\Delta Y$  as a function of the parameter  $R$  at various driver intensities: (a) hydrogen, (b) argon. Other pulse parameters are the same as in Figure 1. (The color version of this figure is included in the online version of the journal.)

The period of the modulation corresponds to a phase change of  $S_P$  by  $\pi$ . Accordingly,  $\delta S_P \approx \pi \delta R = \pi$ , i.e.  $\delta R = 1$ . Hence, we find for the scaling of  $\delta \lambda$  with  $\lambda$

$$\delta \lambda \approx \frac{2\pi c}{I_p + 3U_p}. \quad (7)$$

Equation (7) reproduces the  $\lambda$  dependence of  $\delta \lambda$  quite well (Figure 3).

## 6.2. Comparison between intensity and wavelength variation for short pulses

The parameter  $R$  is a function of both the peak intensity  $I_0$  and the central wavelength  $\lambda_c$  of the driver. An ideal (infinitely) long laser pulse with a flat intensity distribution is characterized by the peak intensity and the (central) wavelength *only*. However, for short, few-cycle laser pulses which are used in contemporary HHG experiments the situation is different. The spectral width  $\Delta\omega$  of the pulse can be large. In the case of the  $\sin^2$ -pulse with a FWHM spread of  $\tau_p = 4$  optical cycles, it is of the order of  $\Delta\lambda/\lambda_c = \Delta\omega/\omega \approx 0.25$  near a central wavelength of 1  $\mu\text{m}$ . At the same time, also an implicit variation of intensity  $\Delta I/I_0$  is present due to the envelope function  $f(t)$ .  $\Delta I$  can be regarded as the temporal intensity sweep,  $\Delta I \approx 0.5I_0$ . A direct comparison in terms of  $R$  of oscillations induced by the function  $R(I_0)$  (via  $U_p(I_0)$ ) and  $R(\lambda_c)$  (via  $U_p(\lambda_c)$ ) is given in Figure 9 for the case of a few-cycle  $\sin^2$  pulse.

In a simple picture one could expect that oscillations in the  $R(\lambda_c)$  curve would be averaged out due to the finite  $\Delta\lambda$  or  $\Delta I$ , similar to channel closing peaks when averaging over the peak intensity  $I_0$  of a monochromatic pulse. That this is *not* the case follows from the fact that the time structure of the electric field is still given by the central wavelength  $\lambda_c$  for the entire pulse. Although the amplitude changes with the pulse envelope on a scale of

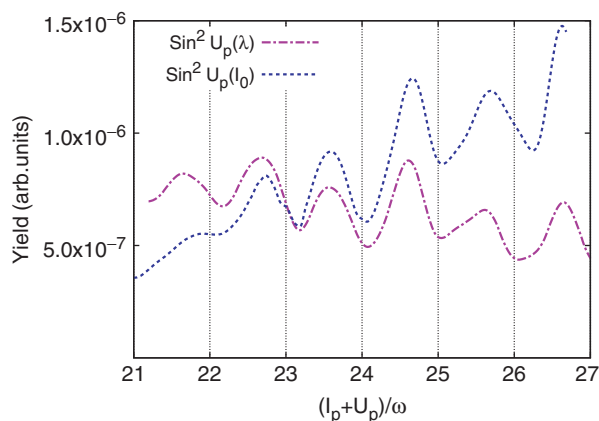


Figure 9. Fluctuations of the harmonic yield  $\Delta Y$  as a function of the parameter  $R$  for hydrogen, comparison of the difference between varying the peak intensity  $I_0$  ( $U_p(I_0)$  and  $\lambda_c = \text{const.}$ ) and the wavelength  $\lambda_c$  ( $U_p(\lambda_c)$  and  $I_0 = \text{const.}$ ). Data for a  $\sin^2$  pulse with a total length of eight cycles is shown. Note, however,  $\tau_p = 4$  cycles in the case of the  $\sin^2$  pulse. Near  $R = 23.1$ , the curves intersect due to identical pulse parameters. (The color version of this figure is included in the online version of the journal.)

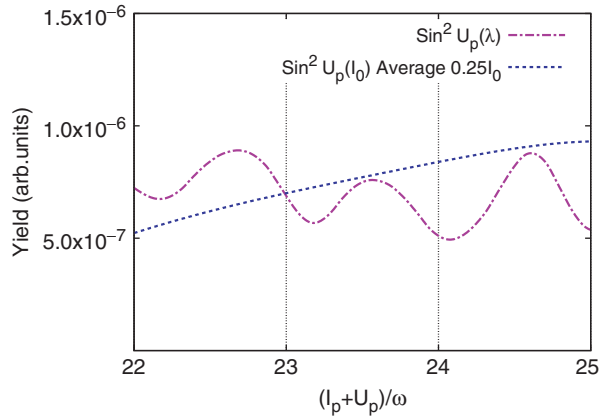


Figure 10. Same as Figure 9, but after intensity averaging over a relative width  $\Delta I_0/I_0$  for the curve  $U_p(I_0)$  comparable to the relative Fourier broadening  $\Delta\lambda/\lambda_c$  of the few-cycle pulse used.

a few optical cycles, this ‘implicit’ averaging over  $\Delta I$  does not destroy the oscillations since it is a coherent process, i.e. that phase information is kept. Accordingly, path interference structures are still visible. Remarkably, such structures can be observed even on a wavelength scale  $\delta\lambda < \Delta\lambda$ .

Along those lines, it is interesting to compare the oscillations induced by the  $\lambda$  dependence of  $U_p(\lambda_c)$  with those by the intensity dependence  $U_p(I_0)$  under the assumption of an equal amount of averaging  $\Delta I_0/I_0 = \Delta\lambda/\lambda_c$ . Such an ‘explicit’ average over the peak intensity  $I_0$  is an incoherent process different from the ‘implicit’ average due to the finite  $\Delta\lambda$ . When employing an intensity averaging with a Gaussian with a FWHM of  $\Delta I_0 = (\Delta\lambda/\lambda_c)I_0$ , oscillations disappear almost completely (Figure 10). By contrast, for a short pulse with  $\Delta\lambda/\lambda_c = 0.25$ , the oscillations are pronounced even though a temporal intensity average (via the envelope) is already included. Therefore oscillations as a function of  $\lambda_c$  are, to some extent, more robust than those as a function of  $I_0$ . Nevertheless, an experimental observation may, inevitably, also contain an average over  $I_0$  due to the spatial intensity distribution in a laser focus. This will have the tendency to smooth out the oscillatory structure. A non-generic spatially flat intensity distribution may serve as a remedy for this problem [9].

## 7. Summary

In conclusion, we have found that the fundamental wavelength dependence of HHG with few-cycle pulses in the single-atom response features surprisingly strong oscillations on fine wavelength scales with modulation periods as small as 6 nm in the mid-infrared regime near  $\lambda = 2\ \mu\text{m}$ . Thus, even a slight change in fundamental wavelength leads to strong variations in the HHG yield. According to a semiclassical analysis based on the SFA, this rapid variation on a fine scale is the consequence of the interference of several rescattering trajectories with long excursion times, confirming the significance of multiple returns of the electron wavepacket [6]. On a large  $\lambda$  scale, apart from the rapid oscillation,

our TDSE results show that the HHG yield at constant intensity decreases as  $\lambda^{-x}$  with  $x \approx 4.8$ – $5.5$  for H and Ar, which is close to the scaling reported in [6]. The oscillations have been found to be stable with respect to variations of the pulse envelope as long as the effective pulse length and thus the number of relevant trajectories remains equal. The present oscillations are related to similar regular enhancements of harmonic yield as a function of the intensity found near channel closings in experiments [9]. The latter have been discussed in the framework of the SFA by employing (infinitely) long, monochromatic driving fields [10]. The detailed structure of the oscillations, however, depends on the given shape of the few-cycle pulse employed, and on the specific atomic potential, which can be accounted for only by a full numerical solution of the TDSE. Furthermore, for short pulses, oscillations of the harmonic yield induced by a variation of  $\lambda$  can be distinguished from those related to a variation of intensity. Although the experimental observability of oscillations in the  $\lambda$  dependence of the yield remains to be analyzed in more detail, preliminary calculations for pulse propagation in one dimension, but accounting for the geometric Guoy phase, show that interference oscillations can persist in loose focus geometry. A spatially flat intensity distribution over the extension of the gas target will be of high importance in order to suppress unwanted averaging effects.

### Acknowledgements

The work was supported by the Austrian ‘Fonds zur Förderung der wissenschaftlichen Forschung’, under Grant No. FWF-SFB016 ‘ADLIS’. K.S. also acknowledges support by the IMPRS-APS program of the MPQ (Germany). K.L.I. gratefully acknowledges financial support by the Precursory Research for Embryonic Science and Technology (PRESTO) program of the Japan Science and Technology Agency (JST) and by the Ministry of Education, Culture, Sports, Science, and Technology of Japan, Grant No. 19686006. K.L.I. would like to thank P. Salières and T. Auguste for illuminating discussions.

### References

- [1] Seres, J.; Seres, E.; Verhoef, A.J.; Tempea, G.; Streltsov, Ch.; Wobrauschek, P.; Yakovlev, V.; Scrinzi, A.; Spielmann, Ch.; Krausz, F. *Nature* **2005**, *433*, 596.
- [2] Hentschel, M.; Kienberger, R.; Spielmann, Ch.; Reider, G.; Milosevic, N.; Brabec, T.; Corkum, P.; Heinzmann, U.; Drescher, M.; Krausz, F. *Nature (London)* **2001**, *414*, 509–513.
- [3] Tsakiris, G.; Tzallas, P.; Charalambidis, D.; Papadogiannis, N.; Witte, K. *Nature (London)* **2003**, *426*, 267–271.
- [4] Sekikawa, T.; Kosuge, A.; Kanai, T.; Watanabe, S. *Nature (London)* **2004**, *432*, 605–608.
- [5] Nabekawa, Y.; Hasegawa, H.; Takahashi, E.J.; Midorikawa, K. *Phys. Rev. Lett.* **2005**, *94*, 043001-1–4.
- [6] Tate, J.; Auguste, T.; Muller, H.G.; Salières, P.; Agostini, P.; DiMauro, L.F. *Phys. Rev. Lett.* **2007**, *98*, 013901-1–4.
- [7] Schiessl, K.; Ishikawa, K.L.; Persson, E.; Burgdörfer, J. *Phys. Rev. Lett.* **2007**, *99*, 253903-1–4.
- [8] Zair, A.; Holler, M.; Guandalini, A.; Schapper, F.; Biegert, J.; Gallmann, L.; Keller, U.; Wyatt, A.S.; Monmayrant, A.; Walmsley, I.A.; et al. *Phys. Rev. Lett.* **2008**, *100*, 143902-1–4.
- [9] Toma, E.S.; Antoine, Ph.; de Bohan, A.; Muller, H.G. *J. Phys. B* **1999**, *32*, 5843–5852.
- [10] Milošević, D.B.; Becker, W. *Phys. Rev. A* **2002**, *66*, 063417-1–14.

- [11] Borca, B.; Starace, A.F.; Flegel, A.V.; Frolov, M.V.; Manakov, N.L. *Phys. Rev. A* **2002**, *65*, 051402(R)-1–4.
- [12] Muller, H.G.; Kooiman, F.C. *Phys. Rev. Lett.* **1998**, *81*, 1207–1210.
- [13] Kulander, K.C.; Schafer, K.J.; Krause, J.L. Time-dependent studies of multiphoton processes. In *Atoms in Intense Laser Fields*; Gavrilin, M., Ed.; Academic: New York, 1992; pp 247–300.
- [14] Tong, X.-M.; Chu, S. *Chem. Phys.* **1997**, *217*, 119–130.
- [15] Schiessl, K.; Persson, E.; Scrinzi, A.; Burgdörfer, J. *Phys. Rev. A* **2006**, *74*, 053412-1–8.
- [16] Lewenstein, M.; Balcou, Ph.; Ivanov, M.Yu.; L’Huillier, A.; Corkum, P.B. *Phys. Rev. A* **1994**, *49*, 2117–2132.
- [17] Salières, P.; Carre, B.; Le Deroff, L.; Grasbon, F.; Paulus, G.G.; Walther, H.; Kopold, R.; Becker, W.; Milosevic, D.B.; Sanpera, A. et al. *Science*. 2001, *292*, 902–905.
- [18] Corkum, P.B. *Phys. Rev. Lett.* **1993**, *71*, 1994–1997.
- [19] Kopold, R.; Becker, W.; Kleber, M.; Paulus, G.G. *J. Phys. B* **2002**, *35*, 217–232.
- [20] Figueira de Morisson Faria, C.; Kopold, R.; Becker, W.; Rost, J.M. *Phys. Rev. A* **2002**, *65*, 023404-1–5.
- [21] Ivanov, M.Yu.; Brabec, T.; Burnett, N. *Phys. Rev. A* **1996**, *54*, 742–745.
- [22] Taieb, R.; Véliard, V.; Wassaf, J.; Manquet, A. *Phys. Rev. A* **2003**, *68*, 033403-1–8.